NANO LETTERS
Cite This: Nano Lett. 2018, 18, 3844−3849
Letter
pubs.acs.org/NanoLett

Spin Direction-Controlled Electronic Band Structure in Two-Dimensional Ferromagnetic CrI_3

Peiheng Jiang,[†,#] Lei Li,[†,#] Zhaoliang Liao,[*,‡,⊥] Y. X. Zhao,[§,∥] and Zhicheng Zhong[*,†]

[†]Key Laboratory of Magnetic Materials and Devices & Zhejiang Province Key Laboratory of Magnetic Materials and Application Technology, Ningbo Institute of Materials Technology and Engineering, Chinese Academy of Sciences, Ningbo 315201, China
[‡]MESA+ Institute for Nanotechnology, University of Twente, P.O. Box 217, 7500 AE Enschede, The Netherlands
[§]National Laboratory of Solid State Microstructures and Department of Physics, Nanjing University, Nanjing 210093, China
[∥]Collaborative Innovation Center of Advanced Microstructures, Nanjing University, Nanjing 210093, China

S *Supporting Information*

ABSTRACT: Manipulating physical properties using the spin degree of freedom constitutes a major part of modern condensed matter physics and is a key aspect for spintronics devices. Using the newly discovered two-dimensional van der Waals ferromagnetic CrI_3 as a prototype material, we theoretically demonstrated a giant magneto band-structure (GMB) effect whereby a change of magnetization direction significantly modifies the electronic band structure. Our density functional theory calculations and model analysis reveal that rotating the magnetic moment of CrI_3 from out-of-plane to in-plane causes a direct-to-indirect bandgap transition, inducing a magnetic field controlled photoluminescence. Moreover, our results show a significant change of Fermi surface with different magnetization directions, giving rise to giant anisotropic magnetoresistance. Additionally, the spin reorientation is found to modify the topological states. Given that a variety of properties are determined by band structures, our predicted GMB effect in CrI_3 opens a new paradigm for spintronics applications.

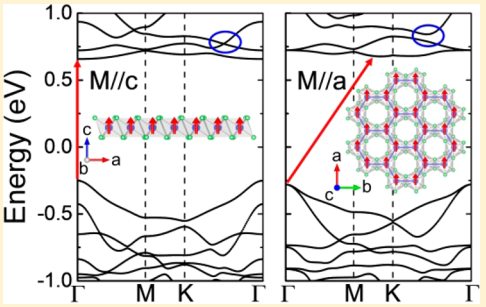

KEYWORDS: *Giant magneto band structure, CrI_3, two-dimensional materials, ferromagnetism*

Novel electronic phases in solid state materials can be driven by the spin degree of freedom due to the delicate interplay between spin, orbital, charge and lattice degrees of freedom.[1] To understand and control the spin is the key to many important electronic devices. In general, the spin ordering structures play a crucial role in determining the physical properties. For example, the metallic phase in correlated manganites is intimately related to long-range ferromagnetic ordering, and a magnetic phase transition from ferromagnetism to para/antiferro-magnetism triggers a metal-to-insulator transition.[2] The phenomenon of multiferroicity results from the coupling between magnetic ordering and electric polarization.[3,4] External magnetic field induced Zeeman spin splitting is usually used to induce magnetic ordering. However, the Zeeman spitting energy is extremely small with only an order of magnitude of 10^{-4} eV under a field of 1 T (see Figure 1a). Besides the Zeeman effect, an applied magnetic field also enforces a reorientation of the spin direction. Since the spin−orbit coupling (SOC) Hamiltonian term $\xi \boldsymbol{L}\cdot\boldsymbol{S}$ depends on the spin direction, the electronic band structure may change when the spin direction is modified by an external magnetic field, in what is called a magneto band-structure (MB) effect. The MB effect can make spin direction a very useful parameter to engineer the band structure and physical properties, in addition to the spin-order controlled properties. Although the importance of MB is very evident and efforts have been made to explore traditional ferromagnetic materials, unfortunately the MB effect of most of the ferromagnetic materials is

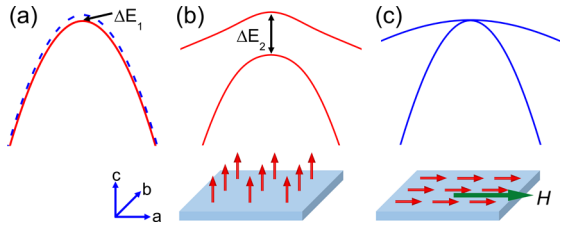

Figure 1. Schematic view of Zeeman effect and giant magneto band structure effect. (a) External magnetic field induced Zeeman splitting of a specific band. The energy splitting ΔE_1 is on an order of 10^{-4} eV under a 1 T magnetic field. (b,c) Calculated band splitting using toy model for a two-dimensional system with (b) magnetization along out-of-plane $\boldsymbol{c}$ axis ($\mathbf{M}//\boldsymbol{c}$), and (c) rearranged magnetization along in-plane $\boldsymbol{a}$ axis ($\mathbf{M}//\boldsymbol{a}$) by applying a magnetic field H. The energy splitting ΔE_2 is on an order of 10^{-1} eV, which is about 10^3 times larger than Zeeman splitting.

Received: March 20, 2018
Revised: May 19, 2018
Published: May 22, 2018

DOI: 10.1021/acs.nanolett.8b01125
Nano Lett. 2018, 18, 3844−3849

too weak to produce interesting properties and functionalities.[5−9]

The big challenge for realizing a pronounced MB effect arises from the fact that many solid state materials have either small spin−orbit coupling or high crystalline symmetry, leading to an intrinsically weak MB effect. In order to make MB materials applicable for practical spintronics applications, a significant change of band structure and thereby functionalities with different spin orientation is required. In this Letter, we establish key criteria to realize such a giant MB effect (GMB) and demonstrate the GMB in the newly discovered two-dimensional (2D) ferromagnet of monolayer CrI_3.[10−19] Our density functional theory calculations show that changing the spin direction of the monolayer CrI_3 remarkably modifies the band structures, including a direct-to-indirect bandgap transition, significant changes of Fermi surfaces, and the modification of topological states. Our results reveal a new approach to manipulate properties by controlling the spin direction.

First, we use a 2D three-p-orbital (p_x, p_y, and p_z) toy model to illustrate the GMB effect. This model is described by the Hamiltonian $H = H_0(k) + \left(\frac{\lambda}{2}\right)\sigma(\theta, \varphi) + \xi \boldsymbol{L}\cdot\boldsymbol{S}$.[20,21] Here, $H_0(k)$ is the paramagnetic tight-binding Hamiltonian with matrix elements $H_{\alpha\beta} = \sum_R t_{\alpha\beta}(\boldsymbol{R})e^{i\mathbf{K}\cdot\boldsymbol{R}}$. $t_{\alpha\beta}(\boldsymbol{R})$ represents a hopping integral from orbital α to orbital β with lattice spacing $\boldsymbol{R}$, and $\mathbf{K}$ is the wave vector. The second term $\left(\frac{\lambda}{2}\right)\sigma(\theta, \varphi)$ describes an exchange splitting λ with magnetization oriented along a specific direction (θ,φ), and $\sigma(\theta,\varphi)$ is the vector of Pauli matrices. The last term is the SOC and the coefficient ξ is the coupling strength. For a 2D ferromagnetic material, it is natural to define the out-of-plane direction as the z-direction and in-plane as (x, y). The ferromagnetic exchange interaction shifts the spin down channel to higher energy, unoccupied states. Meanwhile, the $|p_{z\uparrow}\rangle$ orbital (where ↑ indicates spin up) is split off by 2D confinement effect. Therefore, we mainly focus on $|p_{x\uparrow}\rangle$ and $|p_{y\uparrow}\rangle$ orbitals, which form bands near the Fermi energy. We first consider a situation where the spin is oriented along the out-of-plane direction ($\mathbf{M}//\boldsymbol{c}$). In this case, we have $\langle p_{x\uparrow}|\boldsymbol{L}\cdot\boldsymbol{S}|p_{y\uparrow}\rangle = -i$. As a result, the Hamiltonian has some nonzero off-diagonal mixing terms and the bands at Γ become nondegenerate. A splitting energy of ∼200 meV is found at the Γ point when ξ = 100 meV is used for calculation (see Figure 1b). This energy splitting is indeed induced by SOC, as the splitting vanishes if the SOC is not included (e.g., ξ = 0). In contrast to the situation of $\mathbf{M}//\boldsymbol{c}$, the off-diagonal term $\langle p_{x\rightarrow}|\boldsymbol{L}\cdot\boldsymbol{S}|p_{y\rightarrow}\rangle$ becomes zero (→ denotes spin up channel along in-plane direction) for $\mathbf{M}//\boldsymbol{a}$. Accordingly, the former splitting is removed and bands at Γ are degenerate as shown in Figure 1c.

Switching a magnetic moment from the easy axis ($\mathbf{M}//\boldsymbol{c}$) to the hard axis ($\mathbf{M}//\boldsymbol{a}$) will cost magnetic anisotropic energy (MAE). The MAE is defined as $\Delta E = E_{\rightarrow} - E_{\uparrow}$, where $E_{\rightarrow}$ ($E_{\uparrow}$) is the total energy when the magnetic moment is oriented along the in-plane (out-of-plane) direction. Integrating over all k points in the first Brillouin zone (BZ), the total energy obtained is $E = \sum_i \int_{BZ}\varepsilon_i(k)f(\varepsilon_i - \varepsilon_F)\,dk$, where $f(\varepsilon_i - \varepsilon_F)$ is the Fermi−Dirac distribution, and ε_i and ε_F are energies of the ith band and the Fermi level, respectively.[21] The calculated MAE is on the order of 10^{-3} eV. This fact suggests that a giant change of bands by an order of magnitude of 0.2 eV can be achieved by overcoming an MAE barrier of only ∼10^{-3} eV. This GMB effect which arises from the collective behavior in a 2D ferromagnet with strong SOC is much more significant than the Zeeman effect in a single free electron picture. The large crystalline anisotropy between the in-plane and out-of-plane directions intrinsically exhibited by a 2D ferromagnet is very crucial for the GMB effect. To illustrate the role of symmetry, we extended our model to a nonlayered 3D cubic system where the structure is more isotropic. It is found that the change of the band structure at Γ in the 3D case is not observed because of equivalent spin orientations resulting from the high symmetry.

As indicated by our toy model, we propose three criteria for discovering GMB materials: (i) magnetically coupled electrons to obtain the collective behavior; (ii) strong SOC to induce nonequivalent electronic behavior for different spin orientations; and (iii) a reduced symmetry which has large crystalline anisotropy to maximize SOC anisotropy. These criteria suggest that the most promising candidate is a ferromagnetic material with strong SOC and high crystalline anisotropy.

In light of these criteria, a strong SOC ferromagnet with 2D character, such as a 2D material or layered material which intrinsically exhibits large crystalline anisotropy between the in-plane and out-of-plane directions,[10,22] should be a very promising candidate for demonstrating the GMB effect. While there is inevitable interlayer coupling for 3D layered ferromagnets (for example, the 3D CrI_3 actually exhibits 3D Ising behavior[23,24]), a low dimensional 2D ferromagnet, which has enhanced anisotropy, should be a more ideal system to exhibit larger MB effect. Generally, long-range ferromagnetic order mainly exists in 3d transition metals and their compounds. However, 3d elements have relatively weak SOC and strong SOC can only be found in heavy elements, e.g., 5p and 5d elements. On the other hand, long-range magnetic order is prohibited in 2D materials due to the strong fluctuations at finite temperature according to Mermin-Wagner theorem.[25] Therefore, it is extremely challenging to discover a 2D ferromagnet with strong SOC.

Excitingly, the newly discovered 2D ferromagnet of monolayer CrI_3[10−19] fulfills all of the previously described GMB criteria, providing us with an ideal candidate for realizing the GMB effect. The CrI_3 possesses a graphene-like structure. The Cr atoms form a honeycomb lattice and each Cr is surrounded by six I atoms (see Figure 2).[21] The I^{1-} ion has an orbital configuration of $5s^25p^6$, thereby having very strong SOC. Owing to octahedral symmetry, the five d-orbitals (d_{xy}, d_{xz}, d_{yz}, $d_{x^2-y^2}$, $d_{3z^2-r^2}$) of Cr are split into three t_{2g} orbitals and two e_g orbitals. The three d-electrons ($3d^3$) of Cr^{3+} ion occupy the half-filled t_{2g} orbitals and the e_g orbitals are empty.[26] These orbital configurations and the 90° Cr−I−Cr bond lead to a ferromagnetic superexchange interaction between two nearest neighboring Cr.[27−30] Together with the existence of large magnetic anisotropy (MA) to suppress the spin fluctuations,[25] unique 2D ferromagnetic order can exist in monolayer CrI_3.[10,30] Since its discovery in 2017, many tantalizing magneto-transport and magneto-optic properties have already been realized in monolayer CrI_3.[13,17−19]

There are several types of magnetic anisotropy,[31] for example, shape anisotropy and magnetocrystalline anisotropy. The shape anisotropy favors an in-plane spin orientation for a 2D material. For CrI_3, the magnetocrystalline anisotropy favors an out-of-plane spin orientation.[16] Since the magnetocrystalline anisotropy is larger than shape anisotropy, the magnetocrystalline anisotropy dominates the MA behavior and results in an easy axis along the out-of-plane direction.[10] The MAE of

DOI: 10.1021/acs.nanolett.8b01125
Nano Lett. 2018, 18, 3844−3849

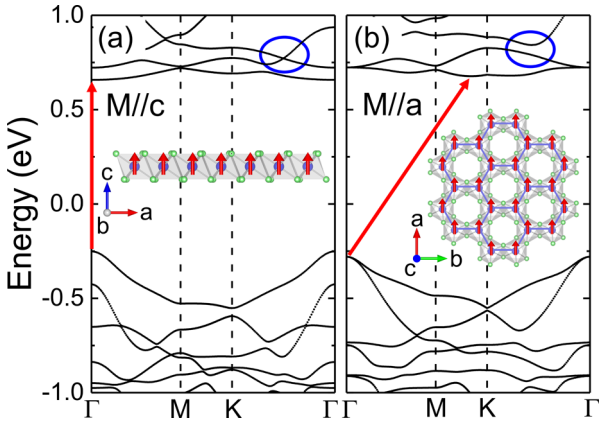

Figure 2. The electronic band structures of monolayer CrI_3. (a) The band structure with magnetic moment along the out-of-plane ***c*** axis. (b) The band structure with magnetic moment along the in-plane ***a*** axis. The red arrows depict the bandgap that is direct with **M**//***c*** and indirect with **M**//***a***. The insets show the side view and top view of the crystal structure with spin oriented along the ***c*** axis and ***a*** axis, respectively. The blue and green balls represent the Cr and I atoms, respectively. The blue circles highlight the band-crossing when **M**//***c***, which becomes gapped when **M**//***a***.

monolayer CrI_3 was calculated using first-principles density functional theory (DFT)[32,33] (see calculation details in the Supporting Information[21]). Our results show that the easy axis is along the out-of-plane direction and the MAE for spins oriented along the in-plane ***a*** axis with respect to the out-of-plane ***c*** axis is 0.98 meV/Cr (see Table 1). Our obtained MAE

Table 1. MAE, Bandgap, and Energy Splitting of Monolayer CrI_3[a]

		bandgap (eV)		Γ split (meV)	
	MAE (meV)	direct	indirect	VBM	CBM
M//***c***	0.00	0.91/1.64 (Γ, Γ)	-----	174.50	64.62
M//***a***	0.98	-----	0.96/1.69 (Γ, M-K)	0.12	0.15

[a]The calculations of MAE and energy splitting are performed with PBE functional, and bandgap calculations are performed with both PBE/HSE functionals.

is quantitatively consistent with the previously reported value of ~0.7 meV/Cr by Zhang et al.[16] The small discrepancy arises from a different calculation method: self-consistence in our calculation versus nonself-consistence in their calculation. The spin direction of CrI_3 can be switched from out-of-plane to in-plane by applying an in-plane external magnetic field to overcome the MAE barrier. The question that arises is whether the spin reorientation can significantly influence the electronic properties. Therefore, we calculated the electronic band structures with the magnetic moment along the ***c*** (**M**//***c***) and ***a*** axis (**M**//***a***), respectively. The electronic band structures for these two different magnetic moment orientations are presented in Figure 2a,b, respectively.

One of the remarkable changes of electronic band structures is a direct-to-indirect bandgap transition when the magnetization is changed from **M**//***c*** to **M**//***a***. In the case of **M**//***c***, the monolayer CrI_3 is a semiconductor with a direct gap of 0.91 eV, as shown in Figure 2a. Since the standard DFT calculations will generally underestimate the bandgap, we further performed a band structure calculation using the Heyd-Scuseria-Ernzerhof (HSE) hybrid functional.[34] The bandgap from the HSE hybrid functional calculation is 1.64 eV.[21] Both the valence band maximum (VBM) and conduction band minimum (CBM) are located at Γ. The splitting energies between the two highest valence bands (VB) and the two lowest conduction bands (CB) at Γ are 174.50 and 64.42 meV, respectively. In addition, the band at Γ near the VBM is mainly formed from the p_x and p_y orbitals of the I atoms.[21] SOC is essential to lift the degeneracy of the bands at Γ, which otherwise become degenerate if the SOC is not included.[21] Such a feature is consistent with the description in our toy model. When the magnetic moment is rotated from the ***c*** axis to the ***a*** axis, the energy splitting disappears for both the VBM and CBM at Γ. Compared to the band structure for **M**//***c***, the VB shifts down while the CB shifts up at Γ. As a result, the CBM is shifted away from Γ to a region between M and K (see Figure 2b) and the bandgap becomes indirect. Therefore, switching the magnetic moment from out-of-plane to in-plane causes a direct-to-indirect bandgap transition.

We propose that such a transition can be easily observed by measuring the photoluminescence. For a direct bandgap material, the electrons that are excited to the CBM can directly relax to the VBM without involving phonon interaction. Therefore, a strong photoluminescence is expected. On the other hand, the photoluminescence will be greatly suppressed for an indirect bandgap material. This significant difference in photoluminescence can be tested by measuring the photoluminescence under an external magnetic field. Recently, Seyler et al. has reported circularly polarized photoluminescence in monolayer CrI_3 under linearly polarized excitation, indicating an effective probe of magnetic order by photoluminescence.[13] In their experiments, only an out-of-plane magnetic field was applied. It will be very interesting to further investigate how the photoluminescence responds to an in-plane magnetic field. Previously, a photoluminescence measurement has been used to confirm a direct-to-indirect bandgap transition in 2D MoS_2, which was triggered by varying the thickness of MoS_2.[35,36] In this regard, CrI_3 can exhibit some advantages over MoS_2, as the photoluminescence in CrI_3 can be reversibly and dynamically controlled by a magnetic field.

Similar to conventional semiconductors such as Si, 2D semiconducting materials can also be doped with vacancies or substitutional impurities. Here, we employ a rigid band shift to investigate the tuning of Fermi surface with spin reorientation in a doped monolayer of CrI_3. Figure 3a,b shows the Fermi surfaces of electron doped monolayer CrI_3 with different magnetization directions. The Fermi surface is found to change from one single ring around the Γ point for **M**//***c*** (Figure 3a) to a shape of a broad bean between M and K for **M**//***a*** (Figure 3b). When CrI_3 is hole doped, the Fermi surface is modified from one single ring (Figure 3c, **M**//***c***) to the double rings (Figure 3d, **M**//***a***) around the Γ point. These changes are correlated to the direct-to-indirect bandgap transition and different energy splitting behavior. Since the Fermi surface plays a crucial role in determining the transport property of a material, the significant change in the Fermi surface of doped monolayer CrI_3 will cause a strong spin direction dependent electronic transport. As a result, a giant anisotropic magnetoresistance (AMR) can be obtained by controlling the direction of remnant magnetization with an external magnetic field. Our Boltzmann transport theory with constant relaxation time

DOI: 10.1021/acs.nanolett.8b01125
Nano Lett. 2018, 18, 3844−3849

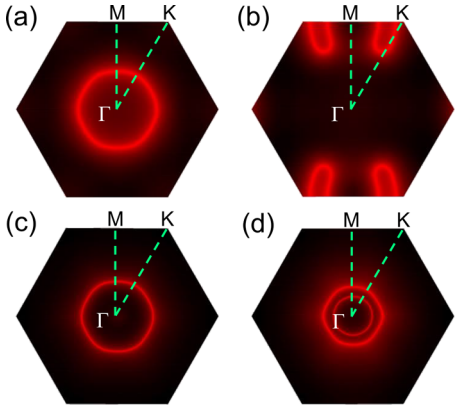

Figure 3. Magnetization direction-dependent Fermi surfaces of CrI_3 doped with 0.2 electrons or holes: (a) electron doping for **M**//***c***; (b) electron doping for **M**//***a***; (c) hole doping for **M**//***c***; (d) hole doping for **M**//***a***.

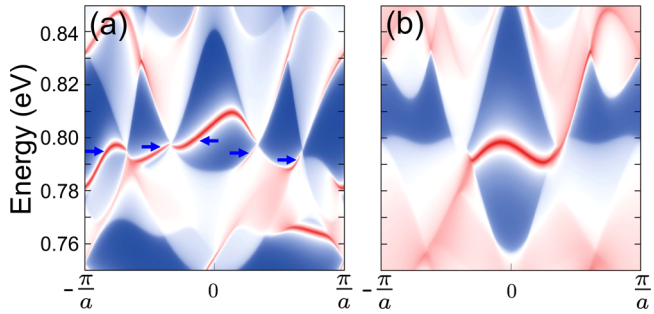

Figure 4. The energy and momentum dependent local DOS (LDOS) on the edge of a semi-infinite sheet of CrI_3 along the zigzag direction. (a) The LDOS for magnetic moment along the out-of-plane ***c*** axis. (b) The LDOS for magnetic moment along the in-plane ***a*** axis. The edge states are indicated by the blue arrows.

calculations[37] demonstrate that the resistivity of a CrI_3 monolayer for perpendicular magnetization ($\rho_\perp$, i.e., ρ(**M**//***c***)) is larger than that for in-plane magnetization ($\rho_\parallel$, i.e., ρ(**M**//***a***)). Here, the current used to measure the resistance is along the in-plane ***a*** axis. This AMR effect, which is due to the change of Fermi surface, is fundamentally different from other kinds of AMR.[38] The AMR ratio is defined as $\Delta\rho/\rho_\perp = (\rho_\perp - \rho_\parallel)/\rho_\perp$. With a slight hole doping, an AMR ratio ~50% is obtained. A larger AMR ratio up to 70% can be achieved in heavily hole doped systems (see Figure S8 in the Supporting Information[21]). Our calculated GMB-driven AMR in CrI_3 is significantly larger than conventional AMR in 3D ferromagnetic materials (which is generally only a few percent[8]), making CrI_3 a promising candidate for spintronics applications. In contrast to traditional GMR devices, which are composed of alternating ferromagnetic and nonmagnetic layers, the utilization of CrI_3 can potentially simplify the device structures by avoiding multilayer stacking and construction. It is worth noting that a similar AMR induced by band structure reconstruction has been recently realized experimentally in Sr_2IrO_4.[39]

Given that the monolayer CrI_3 shares a similar honeycomb structure with graphene and MoS_2, intriguing topological states are expected. Here, we further show that a topological phase transition can be induced by the GMB effect in CrI_3. As indicated by blue circles in Figure 2a, the second and third conduction bands cross each other without opening a gap along the K-Γ direction for **M**//***c***. By mapping out the band structure throughout the whole BZ with a DFT-Wannier-TB method,[40−44] we show that six identical Dirac points exist in the BZ, and each Dirac point is formed by a 2-fold band crossing with linearly leading dispersion; in other words, the coarse-grained Fermions are massless Dirac Fermions. Different from those in graphene with spin degeneracy, these Dirac points consist of only one spin channel. We further confirmed that all the Dirac points have nontrivial $\mathbf{Z}_2$ topological charge by employing the formula $\gamma = \frac{1}{\pi}\oint_C \mathbf{A}(\mathbf{k})\cdot d\mathbf{k} \bmod 2$, where $\mathbf{A}(\mathbf{k}) = i\sum_\alpha \langle u_k^\alpha | \nabla_k | u_k^\alpha \rangle$ is the Berry connection with α labeling the energy bands below the relevant Dirac point, and C is any closed loop locally surrounding it. Due to the nontrivial character, we calculate the corresponding midgap edge states of our system along the zigzag direction as shown in Figure 4a. The edge states all terminate at the projections of the Dirac points as indicated by the blue arrows. There are four projected Dirac points. The first and fourth ones are projected from single Dirac points, but the second and third ones are projected from two Dirac points (see detail in Figure S14 in the Supporting Information[21]). Accordingly, the second and third projected Dirac points are terminated by two edge states. When the magnetization is along the ***a***axis (**M**//***a***), the former band crossing disappears and a bandgap is opened, as indicated by the blue circle in Figure 2b. As the gapped phase is in the vicinity of a Dirac critical point, it is natural to calculate the Chern number by integrating the Berry curvature over the BZ.[21] The calculated Chern number is 1 when up to second conduction bands are considered, indicating that the system is modulated to a Chern topological insulator phase. The corresponding edge states along the zigzag direction are shown in Figure 4b, where a chiral edge band connecting the second and third conduction bands is clearly found, consistent with the bulk-boundary correspondence that the Chern number dictates the number of chiral edge modes. It is worth noting that Hanke et al. recently reported magnetization control of a topological phase transition by spin−orbit torques and Dzyaloshinskii−Moriya interaction.[45]

Although a monolayer CrI_3 is utilized to demonstrate the GMB effect in this letter, our theoretical calculation also suggests the existence of GMB effect in bulk CrI_3 due to its layered structure (see detail in Figure S10 in the Supporting Information[21]). This fact further supports the aforementioned critical role of crystalline anisotropy in inducing GMB. Our results also reveal a slightly different GMB effect in bulk CrI_3 compared to monolayer CrI_3. When **M**//***c***, the splitting energy between the two highest valence bands at Γ for bulk CrI_3 is 94.2 meV, whereas it is 174.5 meV for monolayer CrI_3. In addition, there is no transition from direct band gap to indirect band gap in bulk CrI_3. These differences could be due to the inevitable interlayer coupling in bulk CrI_3. By studying the critical behavior around the magnetic phase transition, recent experiments have demonstrated that the universality class of bulk CrI_3 actually belongs to the 3D Ising model.[23,24]

In summary, we have proposed and demonstrated a giant magneto band structure effect in a 2D ferromagnet of monolayer CrI_3. It is found that changing the spin direction of CrI_3 via an external field can significantly modify electronic band structures, including a direct-to-indirect bandgap transition, as well as modification of the Fermi surface and topological electronic states. Different resistance states can be obtained by switching the magnetization direction of CrI_3. Furthermore, the revealed direct-to-indirect bandgap transition can be used to develop magneto-optoelectronic devices where

DOI: 10.1021/acs.nanolett.8b01125
Nano Lett. 2018, 18, 3844−3849

the photoconductivity can be switched by an external magnetic field. Our results timely provide theoretical insight into the underlying physics of monolayer CrI_3 and should motivate more experiment efforts. Since a variety of properties change with band structure, GMB materials can be used to develop new types of spintronics devices. In contrast to traditional spintronics devices, which require stacking of several magnetic or nonmagnetic materials, GMB materials will be able to simplify device structures and reduce the device size. Finally, we should emphasize that the proposed criteria to discover GMB materials can be applied straightforwardly into the other systems. Thanks to the fast development of materials growth epitaxial techniques, more 2D ferromagnetic materials can be artificially created in ultrathin films or heterostructural interfaces.[46] This provides many great opportunities for us to further explore new GMB materials.

■ ASSOCIATED CONTENT

Supporting Information

The Supporting Information is available free of charge on the ACS Publications website at DOI: 10.1021/acs.nanolett.8b01125.

Details of the DFT-calculated lattice structure, density of states (DOS), band structures, electrical conductivity, magnetic anisotropic energy and additional data (PDF)

■ AUTHOR INFORMATION

Corresponding Authors

*E-mail: z.liao@utwente.nl. Phone: +31 534892860.
*E-mail: zhong@nimte.ac.cn. Phone: +86 574-86681852.

ORCID

Zhaoliang Liao: 0000-0003-1701-9456
Zhicheng Zhong: 0000-0003-1507-4814

Present Address

⊥Materials Science and Technology Division, Oak Ridge National Laboratory, Oak Ridge, Tennessee 37831, USA

Author Contributions

#These authors contributed equally. The manuscript was prepared through the contribution of all authors. All authors have given approval to the final version of the manuscript. Z.Z. supervised the project. P.J. and L.L. calculated and analyzed the results. All authors discussed the results and wrote the manuscript.

Notes

The authors declare no competing financial interest.

■ ACKNOWLEDGMENTS

P.J., L.L., and Z.Z. gratefully acknowledge financial support from the National Key R&D Program of China (2017YFA0303602), 3315 Program of Ningbo, and the National Nature Science Foundation of China (11774360). Calculations were performed at the Supercomputing Center of Ningbo Institute of Materials Technology and Engineering.

■ REFERENCES

(1) Imada, A.; Fujimori, A.; Tokura, Y. *Rev. Mod. Phys.* **1998**, *70*, 1039.
(2) Jin, S.; Tiefel, T. H.; McCormack, M.; Fastnacht, R. A.; Ramesh, R.; Chen, L. H. *Science* **1994**, *264*, 413.
(3) Hill, N. A. *J. Phys. Chem. B* **2000**, *104*, 6694.
(4) Eerenstein, W.; Mathur, N. D.; Scott, J. F. *Nature* **2006**, *442*, 759−65.
(5) Daalderop, G. H. O.; Kelly, P. J.; Schuurmans, M. F. H. *Phys. Rev. B: Condens. Matter Mater. Phys.* **1990**, *41*, 11919−11937.
(6) Velev, J.; Sabirianov, R. F.; Jaswal, S. S.; Tsymbal, E. Y. *Phys. Rev. Lett.* **2005**, *94*, 127203.
(7) Młyńczak, E.; Eschbach, M.; Borek, S.; Minár, J.; Braun, J.; Aguilera, I.; Bihlmayer, G.; Döring, S.; Gehlmann, M.; Gospodarič, P.; Suga, S.; Plucinski, L.; Blügel, S.; Ebert, H.; Schneider, C. M. *Phys. Rev. X* **2016**, *6*, 041048.
(8) McGuire, T.; Potter, R. *IEEE Trans. Magn.* **1975**, *11*, 1018.
(9) Jaoul, O.; Campbell, I. A.; Fert, A. *J. Magn. Magn. Mater.* **1977**, *5*, 23−34.
(10) Huang, B.; Clark, G.; Navarro-Moratalla, E.; Klein, D. R.; Cheng, R.; Seyler, K. L.; Zhong, D.; Schmidgall, E.; McGuire, M. A.; Cobden, D. H.; Yao, W.; Xiao, D.; Jarillo-Herrero, P.; Xu, X. *Nature* **2017**, *546*, 270−273.
(11) Zhong, D.; Seyler, K. L.; Linpeng, X.; Cheng, R.; Sivadas, N.; Huang, B.; Schmidgall, E.; Taniguchi, T.; Watanabe, K.; McGuire, M. A.; Yao, W.; Xiao, D.; Fu, K. -M. C.; Xu, X. *Sci. Adv.* **2017**, *3*, e1603113.
(12) Zheng, F.; Zhao, J.; Liu, Z.; Li, M.; Zhou, M.; Zhang, S.; Zhang, P. *arXiv.org, e-Print Arch., Condens. Matter* **2017**, arXiv:1709.05472.
(13) Seyler, K. L.; Zhong, D.; Klein, D. R.; Gao, S.; Zhang, X.; Huang, B.; Navarro-Moratalla, E.; Yang, L.; Cobden, D. H.; McGuire, M. A.; Yao, W.; Xiao, D.; Jarillo-Herrero, P.; Xu, X. *Nat. Phys.* **2018**, *14*, 277.
(14) Zhang, J.; Zhao, B.; Zhou, T.; Xue, Y.; Ma, C.; Yang, Z. *Phys. Rev. B: Condens. Matter Mater. Phys.* **2018**, *97*, 085401.
(15) Pershoguba, S. S.; Banerjee, S.; Lashley, J. C.; Park, J.; Ågren, H.; Aeppli, G.; Balatsky, A. V. *Phys. Rev. X* **2018**, *8*, 011010.
(16) Zhang, W.-B.; Qu, Q.; Zhu, P.; Lam, C.-H. *J. Mater. Chem. C* **2015**, *3*, 12457−12468.
(17) Wang, Z.; Gutiérrez-Lezama, I.; Ubrig, N.; Kroner, M.; Taniguchi, T.; Watanabe, K.; Imamoğlu, A.; Giannini, E.; Morpurgo, A. F. *arXiv.org, e-Print Arch., Condens. Matter* **2018**, arXiv:1801.08188.
(18) Song, T.; Cai, X.; Tu, M. W. -Y.; Zhang, X.; Huang, B.; Wilson, N. P.; Seyler, K. L.; Zhu, L.; Taniguchi, T.; Watanabe, K.; McGuire, M. A.; Cobden, D. H.; Xiao, D.; Yao, W.; Xu, X. *Science* **2018**, eaar4851.
(19) Klein, D. R.; MacNeill, D.; Lado, J. L.; Soriano, D.; Navarro-Moratalla, E.; Watanabe, K.; Taniguchi, T.; Manni, S.; Canfield, P.; Fernández-Rossier, J.; Jarillo-Herrero, P. *Science* **2018**, eaar3617.
(20) Liao, Z.; Huijben, M.; Zhong, Z.; Gauquelin, N.; Macke, S.; Green, R. J.; Van Aert, S.; Verbeeck, J.; Van Tendeloo, G.; Held, K.; Sawatzky, G. A.; Koster, G.; Rijnders, G. *Nat. Mater.* **2016**, *15*, 425−431.
(21) See Supporting Information.
(22) Gong, C.; Li, L.; Li, Z.; Ji, H.; Stern, A.; Xia, Y.; Cao, T.; Bao, W.; Wang, C.; Wang, Y.; Qiu, Z. Q.; Cava, R. J.; Louie, S. G.; Xia, J.; Zhang, X. *Nature* **2017**, *546*, 265−269.
(23) Lin, G. T.; Luo, X.; Chen, F. C.; Yan, J.; Gao, J. J.; Sun, Y.; Tong, W.; Tong, P.; Lu, W. J.; Sheng, Z. G.; Song, W. H.; Zhu, X. B.; Sun, Y. P. *Appl. Phys. Lett.* **2018**, *112*, 072405.
(24) Liu, Y.; Petrovic, C. *Phys. Rev. B: Condens. Matter Mater. Phys.* **2018**, *97*, 014420.
(25) Mermin, N. D.; Wagner, H. *Phys. Rev. Lett.* **1966**, *17*, 1133−1136.
(26) Lado, J. L.; Fernández-Rossier, J. *2D Mater.* **2017**, *4*, 035002.
(27) Anderson, P. W. *Phys. Rev.* **1950**, *79*, 350−356.
(28) Goodenough, J. B.; Loeb, A. L. *Phys. Rev.* **1955**, *98*, 391−408.
(29) Anderson, P. W. *Phys. Rev.* **1959**, *115*, 2−13.
(30) Wang, H.; Fan, F.; Zhu, S.; Wu, H. *EPL (Europhysics Letters)* **2016**, *114*, 47001.
(31) Dieny, B.; Chshiev, M. *Rev. Mod. Phys.* **2017**, *89*, 025008.
(32) Kresse, G.; Hafner, J. *Phys. Rev. B: Condens. Matter Mater. Phys.* **1993**, *47*, 558−561.
(33) Kresse, G.; Furthmuller, J. *Comput. Mater. Sci.* **1996**, *6*, 15.
(34) Heyd, J.; Scuseria, G. E.; Ernzerhof, M. *J. Chem. Phys.* **2003**, *118*, 8207−8215.

DOI: 10.1021/acs.nanolett.8b01125
Nano Lett. 2018, 18, 3844−3849

(35) Splendiani, A.; Sun, L.; Zhang, Y.; Li, T.; Kim, J.; Chim, C. Y.; Galli, G.; Wang, F. *Nano Lett.* **2010**, *10*, 1271−5.
(36) Mak, K. F.; Lee, C.; Hone, J.; Shan, J.; Heinz, T. F. *Phys. Rev. Lett.* **2010**, *105*, 136805.
(37) Madsen, G. K. H.; Singh, D. J. *Comput. Phys. Commun.* **2006**, *175*, 67−71.
(38) Li, R.-W.; Wang, H.; Wang, X.; Yu, X. Z.; Matsui, Y.; Cheng, Z.-H.; Shen, B.-G.; Plummer, E. W.; Zhang, J. *Proc. Natl. Acad. Sci. U. S. A.* **2009**, *106*, 14224.
(39) Lu, C.; Gao, B.; Wang, H.; Wang, W.; Yuan, S.; Dong, S.; Liu, J.-M. *Adv. Funct. Mater.* **2018**, *28*, 1706589.
(40) Lopez Sancho, M. P.; Lopez Sancho, J. M.; Sancho, J. M. L.; Rubio, J. *J. Phys. F: Met. Phys.* **1985**, *15*, 851.
(41) Marzari, N.; Vanderbilt, D. *Phys. Rev. B: Condens. Matter Mater. Phys.* **1997**, *56*, 12847.
(42) Souza, I.; Marzari, N.; Vanderbilt, D. *Phys. Rev. B: Condens. Matter Mater. Phys.* **2001**, *65*, 035109.
(43) Mostofi, A. A.; Yates, J. R.; Pizzi, G.; Lee, Y.-S.; Souza, I.; Vanderbilt, D.; Marzari, N. *Comput. Phys. Commun.* **2014**, *185*, 2309−2310.
(44) Wu, Q.; Zhang, S.; Song, H.-F.; Troyer, M.; Soluyanov, A. A. *Comput. Phys. Commun.* **2018**, *224*, 405−416.
(45) Hanke, J. P.; Freimuth, F.; Niu, C.; Blugel, S.; Mokrousov, Y. *Nat. Commun.* **2017**, *8*, 1479.
(46) Geim, A. K.; Grigorieva, I. V. *Nature* **2013**, *499*, 419−425.

DOI: 10.1021/acs.nanolett.8b01125
Nano Lett. 2018, 18, 3844−3849